Contact Aging Enhances Adhesion of Micropatterned Silicone Adhesives to Glass Substrates

Jonathan Thiemecke and René Hensel*

The transfer of biological concepts into synthetic micropatterned adhesives has recently enabled a new generation of switchable, reversible handling devices. Over the last two decades, many design principles have been explored that helped to understand the underlying mechanics and to optimize such adhesives for certain applications. An aspect that has been overlooked so far is the influence of longer hold times on the adhesive contacts. Exemplarily, the pull-off stress and work of separation of a micropatterned adhesive specimen are enhanced by factors 3 and 6, respectively, after 1000 min in contact with a glass substrate. In addition to such global measures, the increase of adhesion of all individual micropillars is analyzed. It is found that contact aging varied across the microarray, as it drastically depends on local conditions. Despite great differences on the micropillar scale, the adhesion of entire specimens increased with very similar power laws, as this is determined by the mean contact ageing of the individual structures. Overall, contact aging must be critically evaluated before using micropatterned adhesives, especially for long-term fixations and material combinations that are chemically attractive to each other.

1. Introduction

The handling of components by temporary and reversible adhesion is a crucial element in the automation of industrial production.[1] Micropatterned dry adhesives can fulfill this function and provide unique properties compared to other gripping mechanisms.[2–4] Briefly, the adhesion stress and the work to separate the contact are typically higher when compared to nonpatterned, flat adhesive films, as the elastic deformation during pulling is extended from the crack process zone to the entire length of the micropillar.[5,6] In addition, the work needed to separate the contact is enhanced as the propagating crack is blunted when

J. Thiemecke, Dr. R. Hensel
INM – Leibniz Institute for New Materials
Saarbrücken 66123, Germany
E-mail: rene.hensel@leibniz-inm.de

The ORCID identification number(s) for the author(s) of this article can be found under https://doi.org/10.1002/adfm.202005826.

an individual contact is detached, which then has to be recreated at the next contact to propagate further. Introducing microstructures with high length to diameter ratio inherently opens up a strategy for reversibly switching between low and high adhesive states by compressive buckling of these microstructures.[7,8] Splitting the surface adhering to a substrate into individual contacts further introduces a higher tolerance against defects and misalignment[9–12] and may even generate adhesion to rough surfaces.[13,14]

The adhesion strength of micropatterned adhesives is mainly governed by the geometry of the tip forming the terminal end of each micropillar, as it determines the interfacial stress distribution in the contact.[2] Among others,[15–17] mushroom-shaped tips are frequently used as terminal ends of the micropillars.[18–20] The thin flaps of the mushroom-shaped tips are associated with reduction of the stress singularities at the edges of the adhesive contact, which, in turn, delays separation.[21–23] To improve and optimize micropatterned dry adhesives, intense research has been conducted over the last two decades. Besides modeling of the relevant contact mechanics,[24–26] adhesion experiments combined with in situ observations of detachment events of individual contacts during pull-off have significantly contributed to a better understanding.[15,16,27–29]

A topic that has been overlooked so far is the effect of contact time on the adhesion performance. The time of a micropatterned adhesive in contact with an object can vary greatly between milliseconds or seconds for high cycle rates in robotic handling and minutes to hours for long-term fixtures. Examples of long-term adhesive contacts are the fixture of objects in a batch process such as chemical or physical vapor deposition coatings or the temporary deposition of an object between successive processes. Therefore, variations over time on the adhesive contact are of crucial significance for their design and application. So far, alterations of solid-state contacts over time have been studied in other areas such as frictional contacts,[30,31] the stabilization of colloidal suspensions or granular matter,[32,33] incorporation of inorganic fillers into polymeric matrices,[34] and geophysical research on the origin of earthquakes.[35,36] In general, the phenomena observed are commonly based on the aging of atomic or molecular contacts that, in turn, influence macroscopic properties. Two mechanisms have been proposed to contribute to contact aging: First, the effective contact area increases over time, for example, as a
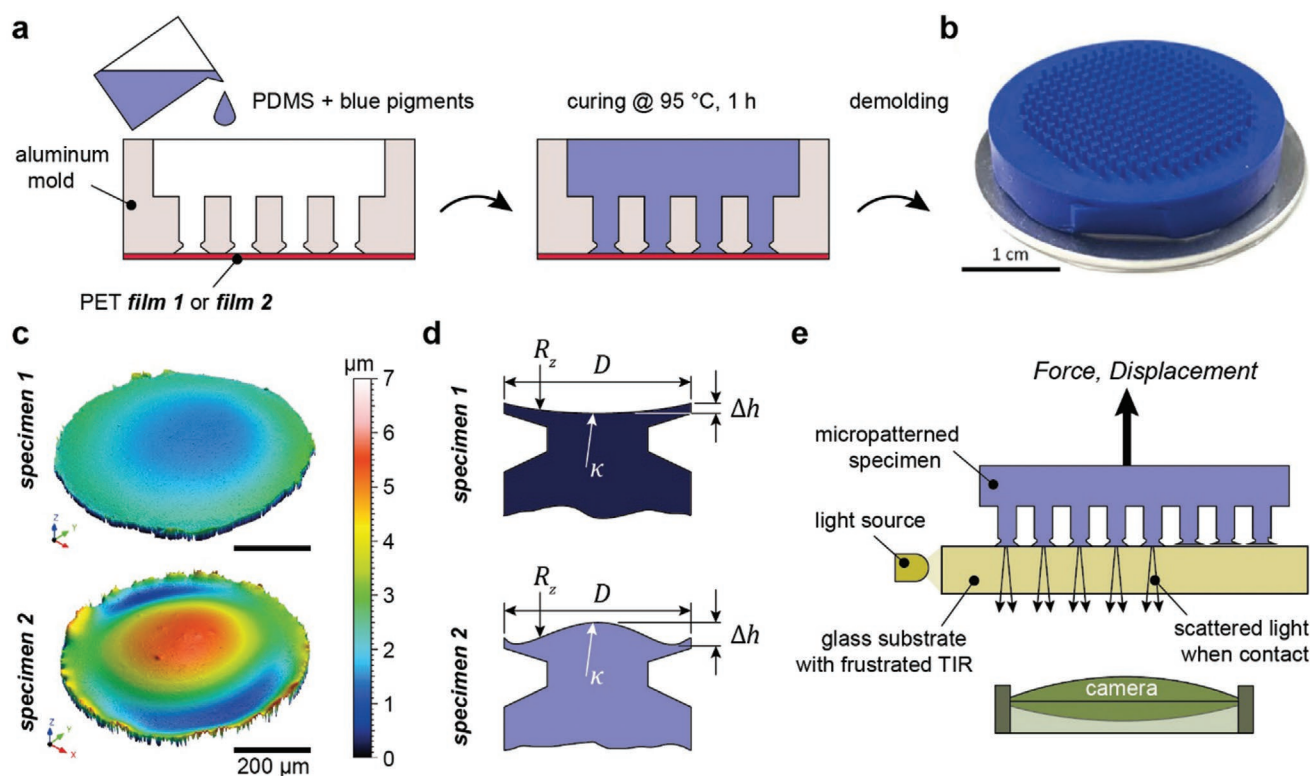
Figure 1. Fabrication and testing of mushroom-shaped microstructures. a) Schematic illustration of the replication process where the polydimethylsiloxane (PDMS) prepolymer together with 10% blue pigment is filled into an aluminum mold. The bottom of the holes is covered with PET film 1 or 2. b) Optical image showing the dimensions of the micropatterned specimens. c) Confocal microscope 3d images of tip surfaces of exemplary micropillars of specimens 1 and 2 showing the surface topography. d) Illustration of the concave (specimen 1) and convex (specimen 2) curved tip surface containing parameters summarized in Table S1, Supporting Information. e) Schematic illustration of the experimental setup. A micropatterned specimen (blue) is brought into contact with a nominally flat glass substrate. The principle of frustrated total internal reflection is used to visualize the individual contacts: Light is scattered only from areas of contact between pillars and substrate. Individual contacts of the specimen with the substrate are recorded in situ using a camera.

result of creep, plastic deformation,[37] capillary condensation,[33] or viscoelastic relaxation. Second, the strength or stiffness of the contact increases, which could result from chemical interactions across the interface, for example, by hydrogen or covalent bond formation[30,38] or an atomic reorientation to reach commensurate configurations.[39] Based on kinetic Monte Carlo simulations, the formation of covalent bonds across the interface was suggested to scale logarithmically with contact time mainly originating from a distribution of reaction energy barriers and elastic interactions between reaction sites.[30,40]

In the present study, we report on enhanced adhesion of micropatterned dry adhesives due to contact aging. We evaluate contact aging on two scales that is on the level of individual micropillars (local scale) and the level of the entire specimen (global scale). This approach provides an insight into statistical effects, since contact aging is drastically dependent on local conditions. In Section 2, we describe the manufacturing of the micropatterned adhesives and the adhesion test procedure, including the principle of frustrated total reflection for visualization of each micropillar in contact with the glass substrate. In Section 3, we report the results: first, the global adhesion of the specimens and, second, the local adhesion of individual pillars including their statistics. Mechanisms leading to interfacial aging of micropatterned adhesives are discussed in Section 4.

2. Experimental Section

2.1. Fabrication of Micropatterned Adhesives

Micropatterned dry adhesives were replicated from polydimethylsiloxane (PDMS, Sylgard 184, Dow Corning, Midland, MI, USA) by using a micropatterned aluminum mold as illustrated in **Figure 1**a.[28] The mold exhibited 241 microscopic holes, which where the negative of the mushroom-shaped micropillars. Diameters of stalks and mushroom tips were about 400 µm and 700 µm, respectively. The bottom of the mold was closed either by the polyethylene terephthalate (PET) film 1 or 2. Both films were slightly deformed, which was then transferred to the tip surfaces of the micropillars during the replication process. Film 1 was a PET film Melinex 401 CW (DuPont, Neu Isenburg, Germany), which was mechanically clamped and expanded thermally at 95 °C during the replication process. The coefficient of thermal expansion of the PET film ($\alpha_{PET} \approx 70 \ 10^{-6} \ K^{-1}$) was higher than the coefficient of thermal expansion of the aluminum mold ($\alpha_{Al} \approx 20 \ 10^{-6} \ K^{-1}$), thus the film expanded into the holes, resulting into the concave curvature of the micropillars of specimen 1 (Figure 1c,d). Film 2 was a PET laminating film Sigma (SIG GmbH, Düsseldorf, Germany), which was thermally bonded to the mold, whereby the film was heated to 120 °C (Präzitherm, Harry Geistigkeit GmbH,

Düsseldorf, Germany) and then bonded to the unheated mold. Film 2 induced convex tip surfaces of the micropillars in the subsequent replication process, as displayed in Figure 1c,d. The PDMS was mixed in a 10:1 ratio of base and curing agent. For better optical contrast, 10 wt% blue pigments (PK 5091, Degussa, Essen Germany) were added to the prepolymer. All components were mixed with 2350 rpm and degassed at 1 mbar for 3 min using a Speed-Mixer (DAC600.2 VAC-P, Hauschild Engineering, Hamm, Germany). The prepolymer mixture was filled into the mold and degassed for 5 min at 1 mbar and, subsequently, cured at 95 °C for 1 h.

Surface topographies of the micropillar tips were measured using confocal microscopy MarSurf CM explorer (Mahr GmbH, Göttingen, Germany) equipped with a 50× objective. Images of the entire tip surface were the result of nine single scans taken in a 3 × 3 matrix that were stitched together. To determine roughness, 10 line scans per surface were post-processed using a 2.5 µm cut-off and a Gaussian filter of 0.08 mm using Explorer software (Mahr GmbH, Göttingen, Germany).

2.2. Adhesion Tests

Adhesion tests were performed with a tensile tester equipped with a 200 N load cell (Inspekt table BLUE, Hegewald&Peschke, Nossen, Germany). A smooth, nominally flat glass substrate (10 mm thick, heat-resistant borosilicate TEMPAX float, MISUMI Europa GmbH, Frankfurt, Germany) was used as substrate. For tests against polystyrene, 1 mm thick polystyrene sheet (taken from square petri dishes, Greiner Bio-One, Frickenhausen, Germany) was glued to the glass substrate. For alignment of the specimen, the substrate was connected to a $\theta - \varphi$ goniometer (MOGO, Owis, Staufen im Breisgau, Germany). In the adhesion measurements, specimen and substrate were brought together with a velocity of 1 mm min^{-1} until a compressive preload of 2 N was reached. After reaching the preload, the specimen was immediately withdrawn with a rate of 1 mm min^{-1} until the compressive force was released ($F = 0$ N). Then, the contact was held for various times before the specimen was retracted with a rate of 10 mm min^{-1}. These tests were performed twice and the mean values were reported. The contact times reported include the time for preloading. Hence, contact times ranged from 10 s (i.e., without rest at $F = 0$ N during retraction) up to 1000 min. Nominal stresses were calculated from forces recorded by the load cell divided by the apparent contact area. The apparent contact area is the real contact area of 92.74 mm^2 (i.e., the number of micropillars multiplied by the area of one mushroom-shaped tip) divided by the areal density of 0.214. We accounted for the elastic deformation of the tensile tester by correcting the motor displacement for the machine stiffness of 785.6 N mm^{-1}. All experiments were performed in a laboratory with controlled temperature and relative humidity at 21 ± 0.2 °C and 50 ± 5%.

2.3. Contact Visualization and Image Analysis

The contact of each micropillar with the substrate was visualized in situ by the principle of frustrated total internal reflection as illustrated in Figure 1e. When a micropillar formed an adhesive contact with the substrate, the light was scattered at the substrate–micropillar interface. Image sequences recorded (DMK33GX236, Imaging Source Europe GmbH, Bremen, Germany) revealed contact formation and detachment of each individual mushroom-shaped micropillar in the entire array. Image sequences were binarized using Fiji[41] such that contact (white) and noncontact (black) areas were identified. The x and y positions for each contact together with the time of attachment and separation were determined using the Analyze Particle tool (Fiji). Position and time data were imported into a MATLAB routine (MathWorks, MA, USA) and correlated with force, time, and displacement data from the adhesion test. For synchronization, the image showing the detachment of the last pillar was attributed to the time when the tensile force relaxed to zero.

3. Results

Micropatterned specimens with mushroom-shaped tips were successfully replicated from polydimethylsiloxane (PDMS) using an aluminum mold and two different polyethylene terephthalate (PET) films to cover the holes at the bottom of the mold (Figure 1 and Figure S1, Supporting Information). As shown in Figure 1c,d, the different films resulted into various surface topographies of the mushroom tips. For surface analyses, five micropillars of each specimen were examined. The surface scans and height profiles are shown in Figures S2 and S3, Supporting Information, and the characteristic values are summarized in Table S1, Supporting Information. Briefly, specimen 1 consisted of micropillars with concave tip curvatures, κ ranging from 6 to 25 m^{-1}, and a height difference between the lowest and the highest point of the tip surface, Δh ranging from 0.7 to 1.9 µm, which is two orders of magnitude smaller than the tip diameter of about 720 µm. The mean peak-to-valley surface roughness, R_z ranged between 43.9 and 55.7 nm. Specimen 2, in contrast, consisted of micropillars with convex tip curvatures ranging from −106.8 to −156.4 m^{-1} with a tip diameter of approx. 700 µm. In addition, their surface was slightly rougher with R_z ranging from 72.8 to 119.0 nm and exhibited a larger Δh between 1.9 and 5.8 µm. In summary, the tip surfaces of specimen 2 were slightly smaller, rougher, and showed a convex curvature compared to the concave curvature of specimen 1. Alongside these tip characteristics, the micropillars of both specimens were of similar length of 1.6 mm and were arranged at the same center-to-center distances of 1.34 mm in a square lattice with 241 micropillars in total.

Adhesion results of the two specimens in contact with the nominal flat glass substrate are displayed in **Figure 2**. In Figure 2a,b, stress–displacement curves are displayed, where the maximum tensile stresses (red squares) are referred to as pull-off stresses, σ_p. For specimen 1, the shape of the stress–displacement curves changed from a bell curve with long tail (10 s) over a trapezoidal (20 min) to a triangularly shaped curve (1000 min). For contact times longer than 20 min, the displacement related to the pull-off stress shifted from values about 0.6 to 1.4 mm, whereas the maximum displacement until complete detachment only slightly enhanced from 1.5 to 1.9 mm. For specimen 2 with much lower adhesion, bell-shaped curves with long tails were found for all contact times. Only for the
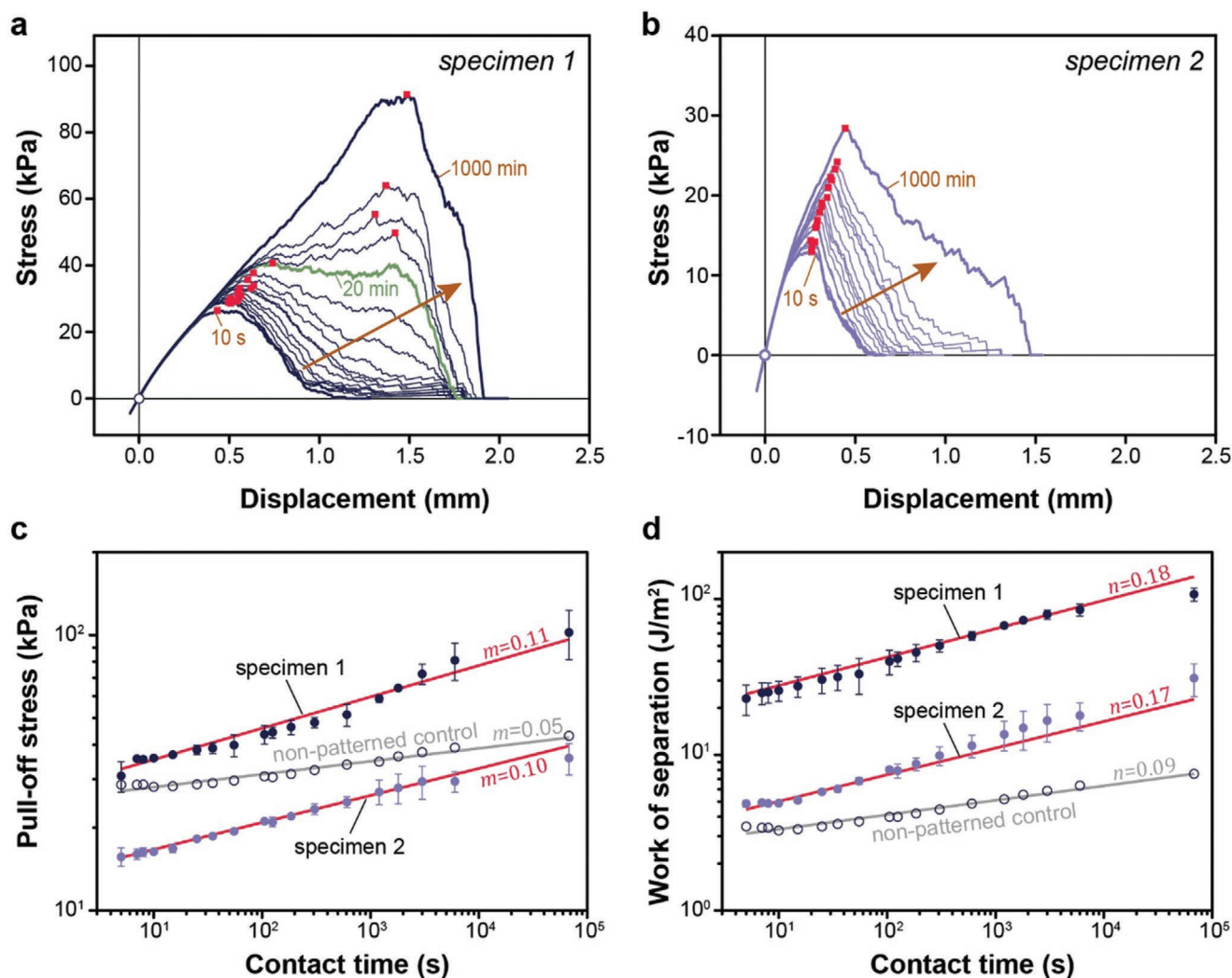
Figure 2. Contact time dependent adhesion results. a,b) Stress versus displacement curves upon different contact times for a) specimen 1 and b) specimen 2. Positive stresses represent tensile stresses. Arrows indicate the increasing contact time from 10 s to 1000 min. The position at which the contact was held is marked by the circle (zero stress). Red squares highlight the pull-off stress. c,d) Log-log plots of c) pull-off stress and d) work of separation versus contact time for specimen 1 (dark blue) and specimen 2 (light blue). Error bars represent the standard deviation. Empty gray circles represent the values of a non-patterned control made of the same material. Red and grey lines represent linear fits with slopes m and n.

1000 min, the tail significantly expanded, indicting a larger fraction of strong micropillars. Figure 2c shows a log-log plot of the pull-off stress as a function of the contact time for the two micropatterned specimens in comparison to a non-patterned, smooth specimen. The pull-off stress of specimens 1 and 2 increased from 30 ± 4 to 102 ± 20 kPa and from 15 ± 1 to 35 ± 5 kPa. It is notable that, for both specimens, the raise of σ_p with contact time, t, followed similar power laws $\sigma_p \approx t^m$ with $m \approx 0.1$, as shown by the linear fits in the log-log plots. In contrast, the pull-off stress of the non-patterned specimen increased only from 28.6 to 43.0 kPa with $m = 0.05$. The area enclosed by the stress–displacement curves (Figure 2a,b) determines the work of separation, w_{sep}, which is displayed in Figure 2d. Their increase over contact time was from 23 ± 5 to 107 ± 10 J m^{-2} and from 5 ± 0.2 to 31 ± 7 J m^{-2} for specimens 1 and 2, respectively. The power laws obtained from linear fits were again similar for both specimens with $n \approx 0.18$. For the

non-patterned specimen, the work of separation increased only twice from 3.5 to 7.5 J m^{-2} with $n = 0.09$. The results imply that the microstructure enhances the contact aging compared to a non-patterned adhesive. In addition, the power laws obtained for the two micropatterned specimens were insensitive to the actual tip geometry, which varied for the two specimens as described above (Figure 1c,d).

In addition to global measurements of the entire specimens, adhesion of the individual micropillars was evaluated using in situ observations of the contacts. **Figure 3**a,b displays the fraction of detached micropillars, N/N_0, in terms of displacement. The limiting cases are $N/N_0 = 0$, at which all micropillars adhered to the substrate and $N/N_0 = 1$, at which all micropillars were detached. With longer contact times, the curves shifted toward larger displacements, indicating an increasing adhesive strength of the individual micropillars, as larger displacements relates to larger strain of the micropillars
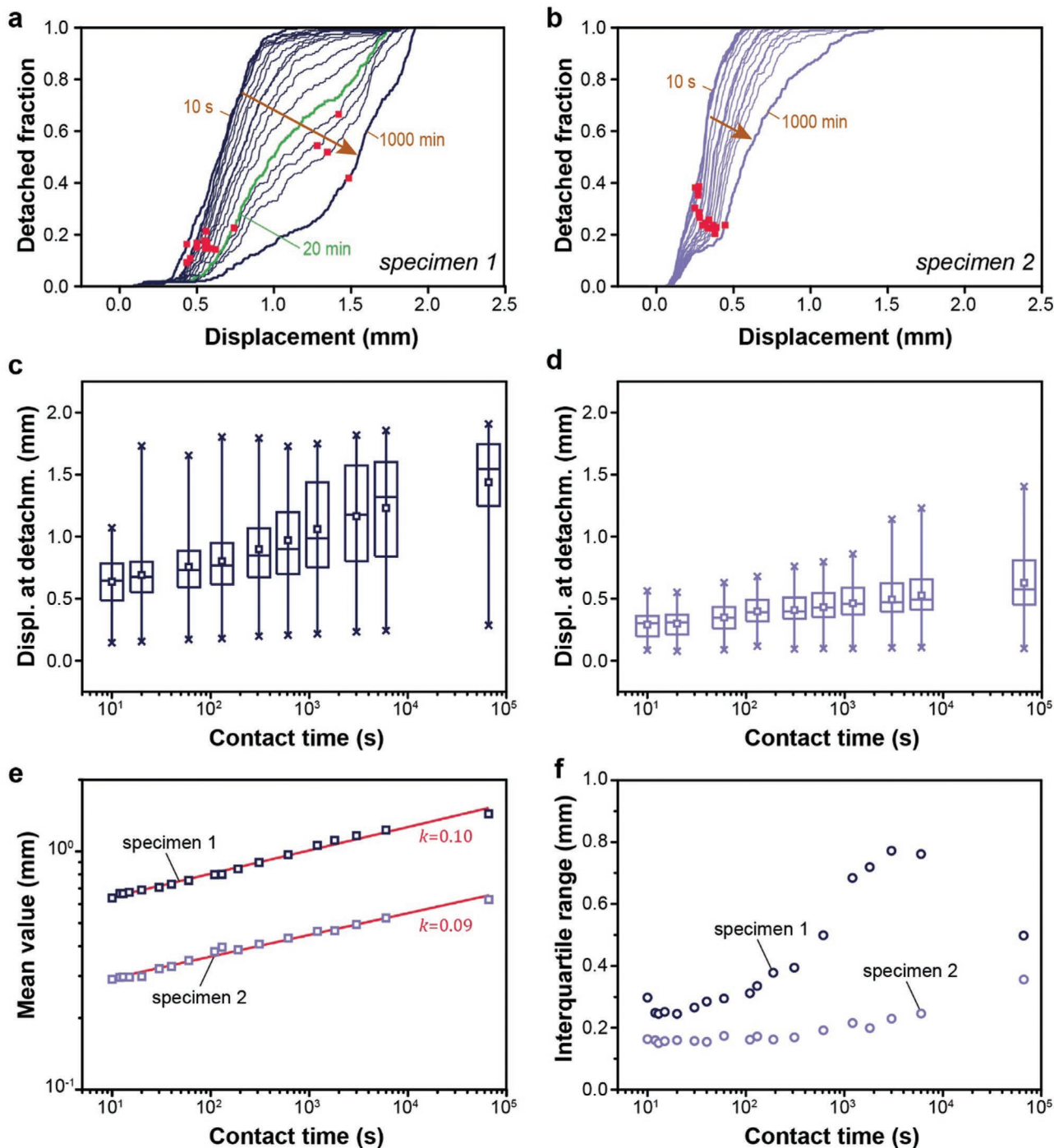
**ADVANCED
SCIENCE NEWS**
www.advancedsciencenews.com

**ADVANCED
FUNCTIONAL
MATERIALS**
www.afm-journal.de

Figure 3. Contact time dependent adhesion results of individual micropillars. a,b) Detached fraction of micropillars, N/N_0, versus displacement, u, for a) specimen 1 and b) specimen 2. Each data point corresponds to the detachment of an individual micropillar. Contact times varied from 10 s to 1000 min. Arrows indicate the increasing contact time from 10 s to 1000 min. Red squares highlight the fraction of detached pillars at pull-off (compare Figure 2a,b). c,d) Box plots showing the distribution of the displacement at detachment u_d as function of the contact time for c) specimen 1 and d) specimen 2. Upper and lower whisker represent 99th and 1st percentile. Squares highlight the mean values. e) Mean values of the displacement at detachment, $\bar{u}_d$, in terms of contact time for specimen 1 (dark blue) and specimen 2 (light blue). Red lines represent linear fits with slope k. f) Interquartile range (i.e., side length of the box in (c,d)) in terms of contact time for specimen 1 (dark blue) and specimen 2 (light blue).

before detachment, which can only be achieved by enhanced adhesion to the substrate. The slope of the curve (in the range $0.2 < N/N_0 < 0.9$) decreased with longer contact times, which

reflects a broader distribution of the adhesive strength across the micropillar array.[29] In addition, all curves in Figure 3b exhibit a kink at $N/N_0 = 0.12$ that indicates about 12% weak
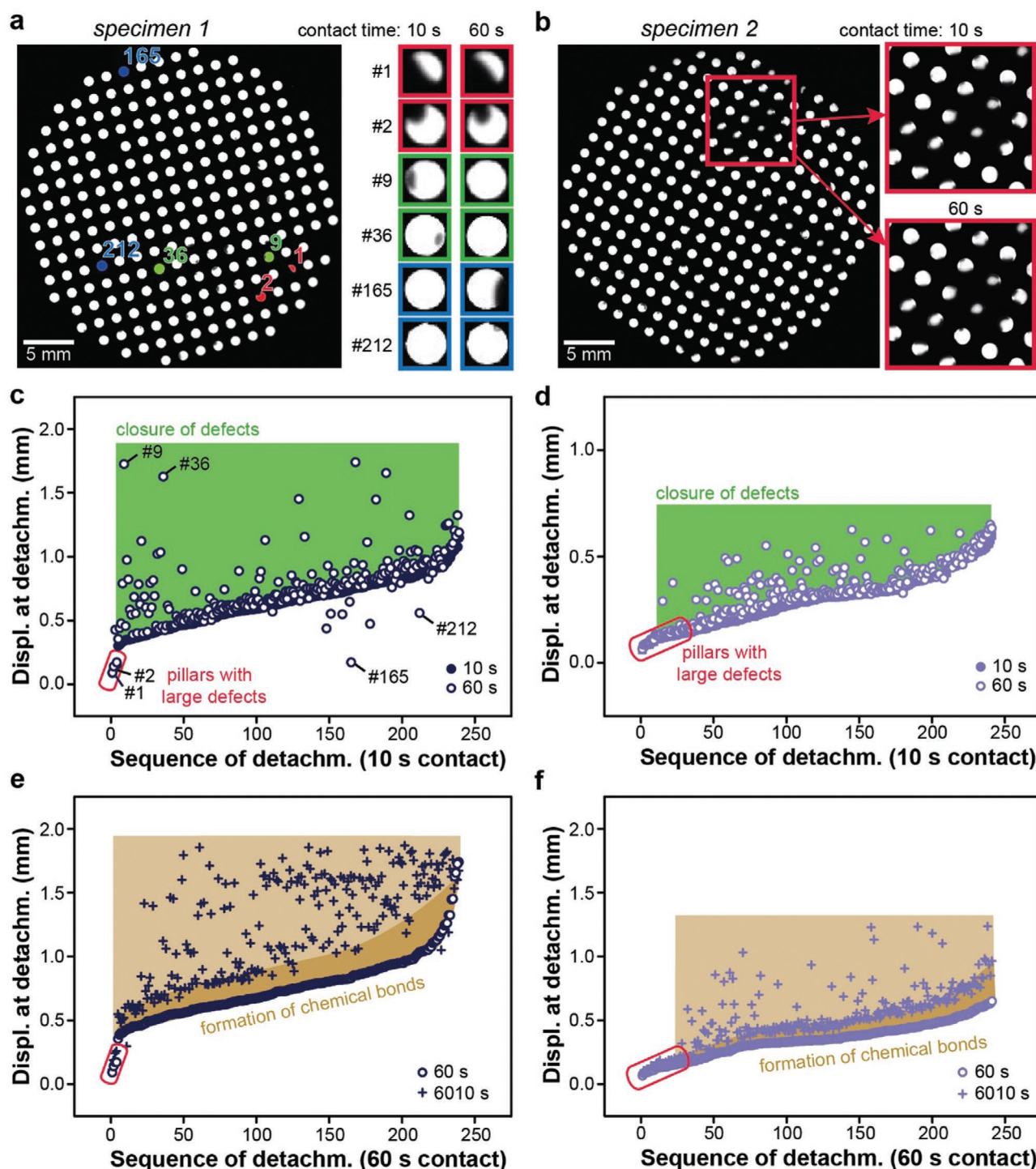
ADVANCED
SCIENCE NEWS
www.advancedsciencenews.com

ADVANCED
FUNCTIONAL
MATERIALS
www.afm-journal.de

Figure 4. Contact aging analysis. a,b) Optical images showing the contact (light gray) upon 10 s for a) specimen 1 and b) specimen 2. Insets in (a) highlight individual contacts upon 10 and 60 s contact time. Insets in (b) highlight exemplary contacts with large defects. c–f) Variation in the sequence of detachment between measurements at different contact times for c,e) specimen 1 and d,f) specimen 2. Filled circles, empty circles, and crosses represent the displacement at detachment of individual micropillars upon 10 s, 60 s, and 6010 s, respectively. In (c) and (d), the sequence of detachment is sorted from weakest to strongest contact upon 10 s contact time. In (e) and (f), the sequence of detachment is sorted from weakest to strongest contact upon 60 s contact time. Contacts with large defects are marked in red. Areas marked green and brown highlight the closure of defects and the formation of chemical bonds along the interface, respectively.

micropillars ($N/N_0 < 0.12$) for specimen 2, whose adhesive properties hardly changed with increasing contact time. The

reason for that were large defects of the mushroom-shaped tips is shown below (compare **Figure** 4b). Similarly, the curves

**ADVANCED
SCIENCE NEWS**
www.advancedsciencenews.com

**ADVANCED
FUNCTIONAL
MATERIALS**
www.afm-journal.de

in Figure 3a show a kink at $N/N_0 = 0.01$, which implies that specimen 1 exhibited a much lower fraction of micropillars with large defects.

By correlating N/N_0 with the stress–displacement curves (Figure 2a,b), the fraction of detached micropillars at the pull-off stress, $N/N_0(\sigma_p)$ could be determined (red squares in Figure 3a,b). For specimen 1, $N/N_0(\sigma_p)$ ranged between 0.1 and 0.2 for contact times between 10 s and 20 min. This implies that between 80 and 90% of the micropillars shared the load at pull-off. For contact times longer than 20 min, $N/N_0(\sigma_p)$ increased to 0.4 and 0.6, that is, only 40–60% of the micropillars shared the load at pull-off. Hence, upon 20 min contact time, a smaller fraction of micropillars was stronger than a larger fraction of microstructure upon shorter contact times. This result is accompanied with the shift from the displacement of ≈0.6 to ≈1.4 mm, at which the pull-off stresses were obtained in the stress–displacement curves (compare Figure 2a). For specimen 2, we observed an inverse trend, where $N/N_0(\sigma_p)$ decreased from 0.4 to 0.2 with increasing contact time (red squares in Figure 3b). Thus, the relative number of micropillars sharing the load at pull-off stress increased from 60% to 80%. In contrast to the global trends presented in Figure 2, the results for both specimens indicate very distinct contact aging of the individual microstructures, which we will examine now in more detail.

The adhesion of individual micropillars can be determined by their displacement at detachment, u_d, as it is related to the maximum tensile strain of the micropillar u_d/H, where $H = 1.6$ mm is the height of the micropillar. Figure 3c,d displays box plots that provide the distribution of u_d for each population of micropillars in terms of contact times. Values of the first (Q1), second (Q2) and third quartile (Q3) increased with contact time for both specimens. Lower whiskers (i.e., 1st percentile of the distribution) remained at similar values, which were 0.16 mm and 0.1 mm for specimens 1 and 2, respectively. In contrast, upper whiskers (i.e., 99th percentile of the distribution) increased from 1.1 to 1.9 mm and from 0.56 to 1.4 mm for specimens 1 and 2, respectively. Figure 3e depicts the increase of mean values, $\overline{u}_d$ as a function of contact time for specimens 1 and 2. Straight lines in the log-log plot indicate the power law $\overline{u}_d \approx t^k$, where $k \approx 0.1$. Figure 3f shows the interquartile range (i.e., side length of the box) for each specimen. For specimen 1, the interquartile range increased from 0.25 to 0.8 mm for a contact time of 50 min. With longer contact times, it decreased to 0.5 mm for 1000 min. Thus, the statistical dispersion of the population first stretched before it squeezed again after 50 min contact time. In other words, contact aging initially broadened the distribution of adhesive performance, whereas after 50 min the distribution became narrower again. The latter was possibly caused by an upper limit of the maximum displacement at detachment, which is in accordance with the upper whisker of constantly 1.9 mm which was insensitive to contact time (Figure 3c). For specimen 2, the interquartile range continuously increased from 0.18 to 0.38 mm without showing a maximum. Here the upper limit was not reached even after 1000 min contact time, as the upper whisker monotonically increased, but was always below 1.9 mm (Figure 3d).

The position of individual micropillars, their sequence of detachment, and the presence of interfacial defects were recorded during the adhesion tests. Figure 4a depicts the contact signature of specimen 1 after 10 and 60 s contact time at zero load just before retraction started. Figure 4b displays similar contact signatures for specimen 2. It should be noted that the different contact times originate from two different experiments. Figure 4c,d compares the displacement at detachment for each micropillar after 60 and 10 s, whereas Figure 4e,f compares the same after 6010 and 60 s contact time. The shorter contact time of these pairs always results in the baseline where all micropillars were sorted from the weakest (left) to the strongest (right) micropillar (measured by the sequence of detachment). The displacement at detachment after the longer contact time was then plotted for the same sequence of detachment. For specimen 1 (Figure 4a), individual contacts #1 and #2 (marked red) show exemplary micropillars with large defects. These contacts detached first and second with the smallest displacement at detachment as shown in Figure 4c. Contacts #9 and #36 show exemplary micropillars with defects in the experiment with 10 s contact time. These contacts detached as 9th and 36th at displacements about 0.4 mm. In the subsequent experiment with 60 s contact time, no defects were visible and u_d improved to about 1.6 mm (green area in Figure 4c). For contacts #165 and #212 (marked blue), we observed opposite trends, as defects were present in the experiment with 60 s contact time, but not in the experiment with 10 s contact time. All examples indicate that the adhesion of individual contacts correlates with the presence of (visible) defects. These defects are present at the very initial contact with the substrate and mostly disappear during compressive preloading, as shown in Figure S4, Supporting Information. The defect closure is accompanied with a rapid increase of the normalized gray value, as depicted in Figure S4d, Supporting Information. Similar trends were observed for specimen 2. It is notable that specimen 2 exhibited about 12% micropillars with significant large tip defects, as shown in Figure 4b. These micropillars detached at displacements ranging between 0.06 and 0.14 mm, which was insensitive to the contact time (Figure 4d).

In addition to short contact times, we compared sequences of detachment for 60 and 6010 s. Figure 4e,f shows that the displacement at detachment of the individual micropillars increased generally by at least 30% with a maximum of 400% for both specimens (brown area in Figure 4e,f). Exceptions were the weakest micropillars with large defects, which improved only slightly (<5%). The strong increase (>100%) of adhesion of individual contacts was randomly distributed and did not correlate to their strength after 60 s contact time, as shown by the strong scattering in Figure 4e,f.

To further clarify where the long-term increase in adhesion originated, we conducted additional tests by replacing the glass substrate with a smooth and flat polystyrene substrate. The mean peak-to-valley roughness of the glass and polystyrene substrate was 1.0 ± 0.2 µm and 1.4 ± 0.2 µm, respectively (Figure S5, Supporting Information). Thus, roughnesses of both substrates were in the same order of magnitude. As shown in **Figure 5**, the variation of the substrate material reduced the pull-off stress and work of separation of specimen 1. Most noticeable, however, was the significantly lower increase in adhesion with longer contact times when adhered to the polystyrene compared to the glass substrate, as reflected in the reduction of the power laws m and n from 0.11 to 0.01 and from 0.18 to 0.05, respectively.

**ADVANCED
SCIENCE NEWS**

www.advancedsciencenews.com

**ADVANCED
FUNCTIONAL
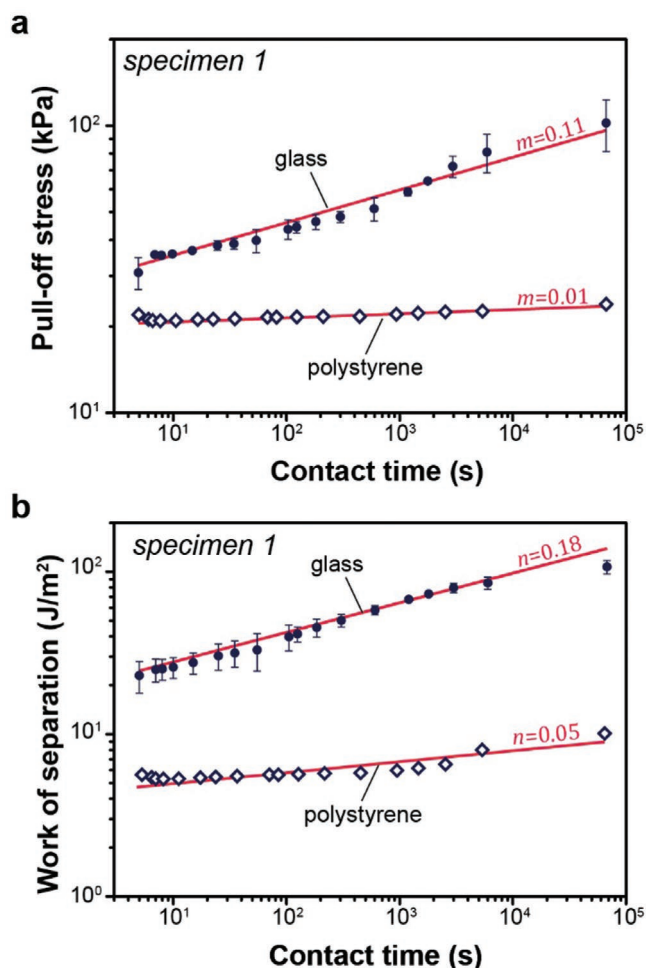MATERIALS**

www.afm-journal.de

Figure 5. Effect of substrate material on contact aging. Logarithmic plots of a) pull-off stress and b) work of separation versus contact time for specimen 1 adhering to glass (circles) and to polystyrene (empty diamonds). Red lines represent linear fits with slopes m and n.

The effect of compressive (−1 and −2 N) and tensile (+1 and +2 N) loading during the time in contact is depicted in **Figure 6**. Qualitatively, pull-off stress and work of separation increased with longer contact times under all conditions irrespective of the loading direction (Figure 6a,b). For short contact times up to 100 s, no clear trends were observed (Figure 6c,d). For longer contact times, both the pull-off stress and work of separation increased more under compressive loading, whereas both increased less under tensile loading. However, there were differences for the two specimens. Sample 1 responded less sensitively to the different loads, since the work of separation increased by 10% under the compressive loads and decreased by about 10% under the tensile loads (Figure 6d). In contrast, for specimen 2, the work of separation at a compressive load of −1 N increased by about 10% and at −2 N by about 40%. At a tensile load of 1 N, the work of separation decreased by about 15% and at 2 N by about 40%. The significant reduction at 2 N was partly caused by the fact that about 30% of the micropillars already detached from the substrate during the contact time. In all other experiments, the number of contacts remained constant over the period of contact time.

4. Discussion

The results obtained provide new insight into the aging of micropatterned adhesive contacts. Different films for closing the aluminum molds for replication led to two specimens with distinct micropillar tip designs. The tips of the micropillars of specimen 2 were slightly smaller, rougher, and showed a convex curvature compared to the concave tip curvature of the micropillars of specimen 1. These parameters together explain the lower (intrinsic) adhesion obtained for specimen 2, which was half in terms of the adhesion stress and a quarter in terms of the work of separation of specimen 1.[13,28] In particular, a concave-curved tip supports higher adhesion as compressive stresses at the edge of the tip counteract dominant tensile stresses during pulling of a micropillar.[16,42] With longer contact times pull-off stresses and works of separation of both specimens increased, which was much larger compared to a non-patterned silicone control. This is most probably caused by the discretization of the adhesive contact of the micropatterned specimens, as each contact has been released individually. In contrast, the non-patterned contact detached from a single defect, which caused a single crack to propagate continuously through the contact. The slopes of the linear functions in the log-log plots and, therefore the power laws $m \approx 0.1$ and $n \approx 0.18$ were similar for the two micropatterned specimens. This result indicates that global aging over contact time ($t > 10$ s) is probably insensitive to specific tip geometries of micropatterned adhesives.

In addition to such a global characterization, we determined the adhesion locally by recording attachment and separation of each individual micropillar. We found that the contacts detached from the substrate gradually, as the adhesion locally varied due to the variations of the micropillar tips, which is in accordance with recent studies by Tinnemann et al. and Booth et al.[28,29] Fractions of micropillars sharing the tensile load at pull-off varied with contact time, but opposite trends were observed whether contact aging supported load sharing or not. Furthermore, box plots of u_d and sequences of detachment varied for each aging experiment, as improved adhesion upon longer contact times scattered drastically. These results clearly demonstrate that aging varied strongly for individual contacts of each specimen. However, the mean value of the displacement at detachment, $\overline{u}_d$ scaled linearly in the log-log plot with similar power laws $k \approx 0.1$ for both specimens. As the work of separation, w_{sep}, is proportional to $\sigma_p \cdot \overline{u}_d$, the scaling of t^n must be proportional to $t^m \cdot t^k$. This gives $n = m + k$, which is in accordance to our results where m and k were 0.1 and n was 0.18. Overall, the aging of the individual contacts varied greatly due to local conditions, but the mean displacement at detachment, which is a measure of the statistical distribution, provides a link from the local micropillar scale to the global scale, that is, the pull-off stress and work of separation of the specimens.

In situ recording of individual contacts provided information about the contact signature. In all experiments, contacts were established by closing interfacial defects upon first contact of the micropillars with the substrate. This process is primarily driven by energy minimization and supported by the compressive preload during attachment.[43] Most contacts were established completely within 10 s, as shown in Figure S4,
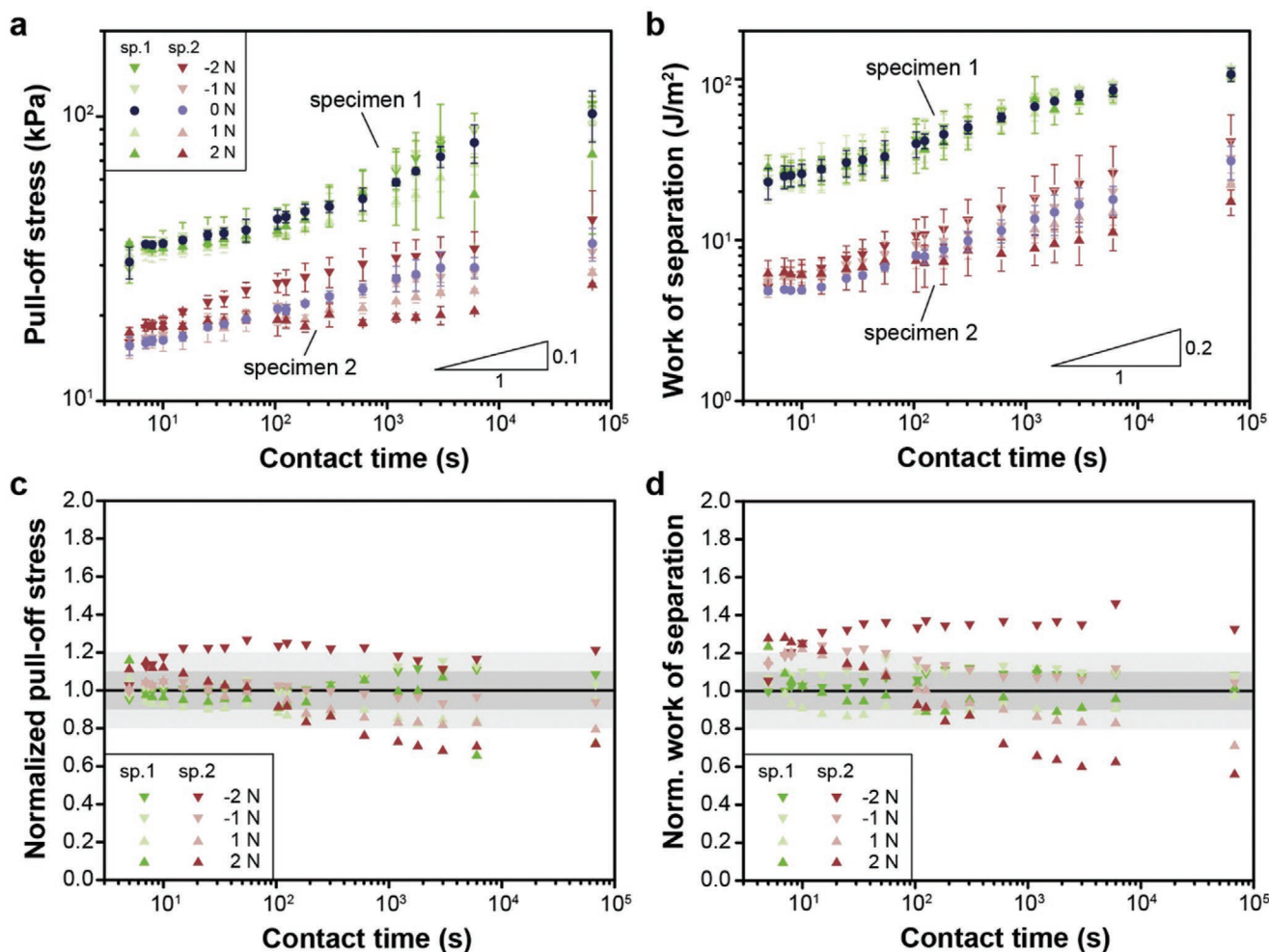
**ADVANCED
SCIENCE NEWS**
www.advancedsciencenews.com

**ADVANCED
FUNCTIONAL
MATERIALS**
www.afm-journal.de

Figure 6. Effect of loading on contact aging. Logarithmic plots of a) pull-off stress and b) work of separation versus contact time for various loading conditions during the hold tests: Triangles pointing downward represent compressive loads of -1 and -2 N and triangles pointing upward represent tensile loads of 1 and 2 N. Circles represent zero load. c,d) Mean values of c) the pull-off stress and d) the work of separation normalized with the unloaded case (0 N).

Supporting Information. However, some defect closures were delayed to tens of seconds. Reasons for the different kinetics can range from varying tip topographies among the micropillars to varying conditions of the glass substrate (such as roughness) at different locations. For example, the rate to close a defect is likely reduced when interfacial stress peaks evolve during closure.[44] Stress peaks can then possibly relax over time due to the slight viscoelastic nature of PDMS with a viscoelastic loss factor, tan δ of 0.1.[45] Another microscopic phenomenon leading to defect closures is the collapse of surface saddle points, which leads to an abrupt coalescence of adjacent contacts.[46,47] Such a collapse could be caused by thermal fluctuations[48] or again by viscoelastic relaxation. Overall, the kinetics of defect closure should depend on the loading conditions during the contact was hold. Accordingly, we found in contact aging experiments at different compressive and tensile loads that the absolute values of the pull-off forces and work of separation increased and decreased, respectively, compared to the unloaded case (Figure 6). However, the power laws differed only slightly for the different scenarios; therefore, defect closure is not the only source for that.

Another mechanism proposed by several groups to explain similar trends in static friction experiments is the formation of chemical bonds across the interface.[2,49,50] For example, two contacting amorphous silica surfaces in a humid environment (such as 50% relative humidity as in our experiments) can form hydrogen bond networks[34] and siloxane (Si–O–Si) bonds across the interface.[31] Siloxane bonds basically result from a condensation reaction of two silanol (Si–OH) groups or from the reaction of a silanol with a siloxane group or two siloxane groups located oppositely across the interface.[50,51] Such bonds are likely to form in a similar manner between the polydimethylsiloxane elastomer and the borosilicate glass substrate used in our experiments (**Figure 7**). To test the hypothesis, experiments were repeated, at which the glass substrate was replaced by a polystyrene substrate (Figure 5). Adhesion improved barely to the polystyrene substrate even upon a contact time of 1000 min, mainly due to lack of covalent bonds, as polystyrene is apolar and relatively chemically inert.

In general, covalent bonds are stronger than van der Waals interactions, which inherently increase the adhesion energy and reduce the distance between the PDMS elastomer and the
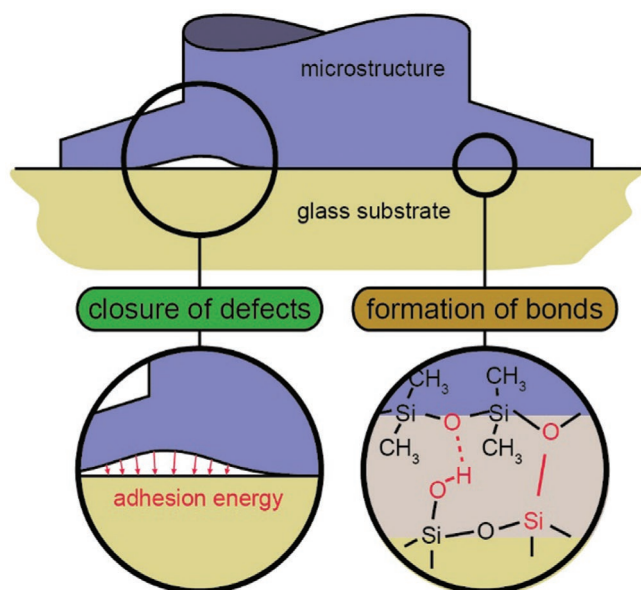
Figure 7. Contact aging mechanisms. Illustration of two mechanisms improving adhesion of silicone micropillars to silica glass with longer contact times: (left) improved effective contact area by the closure of defects and (right) enhanced contact strength by formation of hydrogen and covalent bonds.

glass substrate that, in turn, can further promote the closure of defects. Furthermore, the formation of chemical bonds inherently leads to irreversible contacts, which then break at a critical tensile load. However, when the sum of chemical bonds exceeds the material strength, the contact will likely separate via cohesive rupture. An example of irreversible detachment is depicted in Figure S6, Supporting Information, where, upon pull-off, residues were found after 7 days of contact with a glass substrate. Therefore, chemical aging has to be critically evaluated before applying micropatterned adhesives for long-term fixations. Furthermore, we should note that several silicone materials with different amounts of additives are commercially available to produce micropatterned adhesives.[52] Such differences in the chemical nature of the adhesives can significantly affect the contact aging properties.[34]

Finally, we come back to the large scattering of adhesion of individual contacts, which, for example, after 6010 s contact time, varied greatly between 30% and 400% (compare Figure 4e,f). This finding relates most probably to locally dependent chemical and topographical variations in the repeated adhesion tests, which is in accordance with molecular dynamics and kinetic Monte Carlo simulations by Liu et al. and Li et al.[30,38] They demonstrated nonlinearly scaling of the contact strength with the concentration of interfacial bonds and proposed that elastic interactions among adjacent bonds induces variations of the energy barrier. This can be caused by an inhomogeneous distribution of chemically attractive sites or surface roughness leading to differences of interfacial stresses and local variations in the position of the micropillars during repeated adhesion tests.[40] Overall, the power laws obtained in our study most likely result from bond formations that varied locally between repeated experiments.

5. Conclusions

Enhanced adhesion of micropatterned silicone adhesives due to contact aging was investigated using an in situ method for visualizing individual contacts. This approach provided insight into aging phenomena on the local (micropillars) and global (specimen) scale. Local variations led to a distribution of the adhesion performance, where the mean adhesion value of the individual adhesive contacts represents the enhanced adhesion of the entire specimen. The following conclusions can be drawn:

- Two key mechanisms help to improve adhesion over time as illustrated in Figure 7: 1) Immediately when the micropatterned adhesive touches the substrate, adhesion energy governs the closure of defects that improves the contact area. It is typically quite fast within a few seconds as polydimethylsiloxane exhibits low viscoelasticity. 2) Upon defect closure, chemical bonds potentially form across the interface. These bonds are stronger than van der Waals interactions leading to improved adhesion performance with longer contact times.
- The mean displacement at detachment of individual micropillars provides a measure of the statistics and links it to the pull-off stress and work of separation of the entire specimens. Therefore, the power laws obtained from log-log plots, resulted from the contact aging distribution of the individual contacts.
- Contact aging of the specimens is sensitive to compressive and tensile loading during the contact time, as the load increases or reduces the real contact area for non-flat contacts. However, power laws describing the trends of the pull-off stress and work of separation with contact time remained similar.
- Chemically inert surfaces or large predetermined interfacial defects can prevent or reduce contact aging effects.

Taken together, this study demonstrates the importance of long-term experiments that can lead to improved adhesion. This is particularly important for applications with adhesive contact times in the order of minutes and hours, since in the worst case, the formation of covalent bonds can lead to a loss of reversibility and residues on the counter surface after detachment.

Supporting Information

Supporting Information is available from the Wiley Online Library or from the author.

Conflict of Interest

The authors declare no conflict of interest.

Keywords

[1] J. Frohm, V. Lindström, M. Winroth, J. Stahre, *Ergonomia* **2008**, *2008*, 31.

[2] R. Hensel, K. Moh, E. Arzt, *Adv. Funct. Mater.* **2018**, *28*, 1800865.

[3] M. Kamperman, E. Kroner, A. Del Campo, R. M. McMeeking, E. Arzt, *Adv. Eng. Mater.* **2010**, *12*, 335.

[4] E. Arzt, S. Gorb, R. Spolenak, *Proc. Natl. Acad. Sci. U. S. A.* **2003**, *100*, 10603.

[5] N. J. Glassmaker, A. Jagota, C.-Y. C.-Y. Hui, W. L. Noderer, M. K. Chaudhury, *Proc. Natl. Acad. Sci. U. S. A.* **2007**, *104*, 10786.

[6] C.-Y. Hui, N. J. Glassmaker, T. Tang, A. Jagota, *J. R. Soc., Interface* **2004**, *1*, 35.

[7] V. Tinnemann, E. Arzt, R. Hensel, *J. Mech. Phys. Solids* **2019**, *123*, 20.

[8] D. R. Paretkar, M. D. Bartlett, R. McMeeking, A. J. Crosby, E. Arzt, *J. Adhes.* **2013**, *89*, 140.

[9] G. J. Amador, T. Endlein, M. Sitti, *J. R. Soc., Interface* **2017**, *14*, 20170134.

[10] W. Bin Khaled, D. Sameoto, *Bioinspiration Biomimetics* **2013**, *8*, 044002.

[11] M. Bacca, J. A. Booth, K. L. Turner, R. M. McMeeking, *J. Mech. Phys. Solids* **2016**, *96*, 428.

[12] J. A. Booth, M. Bacca, R. M. McMeeking, K. L. Foster, *Adv. Mater. Interfaces* **2018**, *5*, 1800272.

[13] V. Barreau, R. Hensel, N. K. Guimard, A. Ghatak, R. M. McMeeking, E. Arzt, *Adv. Funct. Mater.* **2016**, *26*, 4687.

[14] C.-Y. Hui, N. J. Glassmaker, A. Jagota, *J. Adhes.* **2005**, *81*, 699.

[15] S. C. L. Fischer, E. Arzt, R. Hensel, *ACS Appl. Mater. Interfaces* **2017**, *9*, 1036.

[16] Y. Wang, V. Kang, E. Arzt, W. Federle, R. Hensel, *ACS Appl. Mater. Interfaces* **2019**, *11*, 26483.

[17] Y. Wang, H. Tian, J. Shao, D. Sameoto, X. Li, L. Wang, H. Hu, Y. Ding, B. Lu, *ACS Appl. Mater. Interfaces* **2016**, *8*, 10029.

[18] D. Yu, D. Beckelmann, M. Opsölder, B. Schäfer, K. Moh, R. Hensel, P. de Oliveira, E. Arzt, *Materials* **2019**, *12*, 97.

[19] L. Heepe, A. E. Kovalev, M. Varenberg, J. Tuma, S. N. Gorb, *Theor. Appl. Mech. Lett.* **2012**, *2*, 014008.

[20] S. Gorb, M. Varenberg, A. Peressadko, J. Tuma, *J. R. Soc., Interface* **2007**, *4*, 271.

[21] A. V. Spuskanyuk, R. M. McMeeking, V. S. Deshpande, E. Arzt, *Acta Biomater.* **2008**, *4*, 1669.

[22] R. G. Balijepalli, M. R. Begley, N. A. Fleck, R. M. McMeeking, E. Arzt, *Int. J. Solids Struct.* **2016**, *85–86*, 160.

[23] L. Heepe, S. N. Gorb, *Annu. Rev. Mater. Res.* **2014**, *44*, 173.

[24] M. Ciavarella, J. Joe, A. Papangelo, J. R. Barber, *J. R. Soc., Interface* **2019**, *16*, 20180738.

[25] M. H. Müser, W. B. Dapp, R. Bugnicourt, P. Sainsot, N. Lesaffre, T. A. Lubrecht, B. N. J. Persson, K. Harris, A. Bennett, K. Schulze, S. Rohde, P. Ifju, W. G. Sawyer, T. Angelini, H. A. Esfahani, M. Kadkhodaei, S. Akbarzadeh, J. J. Wu, G. Vorlaufer, A. Vernes, S. Solhjoo, A. I. Vakis, R. L. Jackson, Y. Xu, J. Streator, A. Rostami, D. Dini, S. Medina, G. Carbone, F. Bottiglione, L. Afferrante, J. Monti, L. Pastewka, M. O. Robbins, J. A. Greenwood, *Tribol. Lett.* **2017**, *65*, 118.

[26] N. A. Fleck, S. N. Khaderi, R. M. McMeeking, E. Arzt, *J. Mech. Phys. Solids* **2017**, *101*, 30.

[27] L. Heepe, A. E. Kovalev, A. E. Filippov, S. N. Gorb, *Phys. Rev. Lett.* **2013**, *111*, 104301.

[28] V. Tinnemann, L. Hernández, S. C. L. Fischer, E. Arzt, R. Bennewitz, R. Hensel, *Adv. Funct. Mater.* **2019**, *29*, 1807713.

[29] J. A. Booth, V. Tinnemann, R. Hensel, E. Arzt, R. M. McMeeking, K. L. Foster, *J. R. Soc., Interface* **2019**, *16*, 20190239.

[30] Y. Liu, I. Szlufarska, *Phys. Rev. Lett.* **2012**, *109*, 186102.

[31] G. Vigil, Z. Xu, S. Steinberg, J. Israelachvile, *J. Colloid Interface Sci.* **1994**, *165*, 367.

[32] F. Bonacci, X. Chateau, E. M. Furst, J. Fusier, J. Goyon, A. Lemaître, *Nat. Mater.* **2020**, *19*, 775.

[33] L. Bocquet, E. Charlaix, S. Ciliberto, J. Crassous, *Nature* **1998**, *396*, 735.

[34] J. V. Degroot, C. W. Macosko, *J. Colloid Interface Sci.* **1999**, *217*, 86.

[35] C. D. Rowe, K. Lamothe, M. Rempe, M. Andrews, T. M. Mitchell, G. Di Toro, J. C. White, S. Aretusini, *Nat. Commun.* **2019**, *10*, 320.

[36] C. A. Thom, R. W. Carpick, D. L. Goldsby, *Geophys. Res. Lett.* **2018**, *45*, 13306.

[37] T. Baumberger, C. Caroli, *Adv. Phys.* **2006**, *55*, 279.

[38] A. Li, Y. Liu, I. Szlufarska, *Tribol. Lett.* **2014**, *56*, 481.

[39] M. Feldmann, D. Dietzel, A. Tekiel, J. Topple, P. Grütter, A. Schirmeisen, *Phys. Rev. Lett.* **2016**, *117*, 025502.

[40] Z. Li, L. Pastewka, I. Szlufarska, *Phys. Rev. E* **2018**, *98*, 023001.

[41] J. Schindelin, I. Arganda-Carreras, E. Frise, V. Kaynig, M. Longair, T. Pietzsch, S. Preibisch, C. Rueden, S. Saalfeld, B. Schmid, J. Y. Tinevez, D. J. White, V. Hartenstein, K. Eliceiri, P. Tomancak, A. Cardona, *Nat. Methods* **2012**, *9*, 676.

[42] S. C. L. Fischer, K. Groß, O. T. Abad, M. M. Becker, E. Park, R. Hensel, E. Arzt, *Adv. Mater. Interfaces* **2017**, *4*, 1700292.

[43] K. L. Johnson, K. Kendall, A. D. Roberts, *Proc. R. Soc. A Math. Phys. Eng. Sci.* **1971**, *324*, 301.

[44] R. M. McMeeking, L. Ma, E. Arzt, *Adv. Eng. Mater.* **2010**, *12*, 389.

[45] S. C. L. Fischer, K. Kruttwig, V. Bandmann, R. Hensel, E. Arzt, *Macromol. Mater. Eng.* **2017**, *302*, 1600526.

[46] W. B. Dapp, M. H. Müser, *EPL* **2015**, *109*, 44001.

[47] V. A. Yastrebov, G. Anciaux, J.-F. Molinari, *Tribol. Lett.* **2014**, *56*, 171.

[48] M. Vorholzer, J. G. Vilhena, R. Perez, E. Gnecco, D. Dietzel, A. Schirmeisen, *Phys. Rev. X* **2019**, *9*, 041045.

[49] K. Autumn, M. Sitti, Y. A. Liang, A. M. Peattie, W. R. Hansen, S. Sponberg, T. W. Kenny, R. Fearing, J. N. Israelachvili, R. J. Full, *Proc. Natl. Acad. Sci. U. S. A.* **2002**, *99*, 12252.

[50] J. N. Israelachvili, *Intermolecular and Surface Forces*, (3rd ed.), Elsevier, New York **2011**.

[51] M. Wang, F. Duan, X. Mu, *Langmuir* **2019**, *35*, 5463.

[52] A. Simaite, M. Spenko, *Bioinspiration Biomimetics* **2019**, *14*, 046005.